2012 IEEE International Conference on Green Computing and Communications, Conference on Internet of Things, and Conference on Cyber, Physical and Social Computing

Autonomous Recognition of Emergency Site by Wearable Sensors

Masaki Inokuchi† Takamasa Higuchi† Hirozumi Yamaguchi†,‡ Teruo Higashino†,‡
†Graduate School of Information Science and Technology, Osaka University,
1-5 Yamadaoka, Suita, Osaka 565-0871, Japan,
‡ Japan Science and Technology Agency, CREST,
{ i-masaki, t-higuti, h-yamagu, higashino }@ist.osaka-u.ac.jp

***Abstract*—To support rescue activities of first responders is crucial at disaster sites. Especially, provisioning location and situation information is indispensable for those first responders to efficiently rescue injured people in unknown places with a lot of buildings such as private properties (like factories) and university campus. In such an extreme situation, seamless indoor/outdoor maps will be of substantial aid for the first responders. In this paper, we propose a method of creating an indoor/outdoor map by a first responder team. We assume some of them are equipped with range scanners and all the members have GPS and WiFi devices. Then the presence of obstacles and movable areas is estimated by combining information from different sources (like GPS, WiFi and range scanners) with different confident levels. Since these confident levels depend on scenarios and environments, we design an "adaptive information fusion" algorithm that automatically estimates the confident levels to optimize the precision of the generated map. We have demonstrated our method in several experiments with real sensor data.**

***Keywords*-map generation, indoor/outdoor map, range scanner, position information**

I. Introduction

As every country has a risk of disasters like big earthquakes and serious accidents which unfortunately happen from time to time, rescue teams are organized and well-trained to engage in rescue operations such as finding injured people who need emergency help. Since those people have been wounded due to furniture fall-down or some other reasons, they often cannot move by themselves. To help all those injured, rescue team members need to seek the whole disaster area where they may not be familiar to. Although digital maps (like Google maps) may be available to the team members, they do not provide detailed information on shapes and locations of buildings if the site is private property. Furthermore, when the buildings have collapsed due to earthquakes, it gets much harder for the team members to recognize the situation. To make matters worse, digital indoor floor maps are not usually available. For more efficient search that covers the whole region including indoor space at unknown sites, team members need to share an indoor/outdoor digital map with sufficient accuracy.

There is national project funded by the Japanese ministry [1] to develop a sensing system that collects vital signs of injured people by attaching small wireless sensor nodes to their fingertips. It enables to monitor their vital conditions in such situations that many people are injured but there are not sufficient human resources to rescue all those people simultaneously. Based on a number of discussions with rescue team members and doctors through this project, Minamimoto et. al. have reached the solution in previous literature [2], [3] where position and ad-hoc communication logs are collected via GPS and WiFi devices of the team members, and then analyzed to obtain estimation of building shapes and locations. The motivation to this approach is requirement for simple and efficient map estimation at such unknown sites.

However, there are still other needs which are also very important to support rescue activities. Firstly, indoor map estimation is quite mandatory as well as outdoor maps. For example, in some accidents, carbon monoxide will be generated and will cause serious damage to indoor people. Big earthquakes may also cause a lot of indoor victims due to collapse of stuff such as office furniture and shelves at shops. Secondly, there is a certain limit on sensing capabilities when only wireless and GPS devices are utilized. Actually, wireless beacons substantially help to obtain coarse-grained 2D view of building shape and location, since buildings between two nodes block the beacons with high probabilities [2], [3]. However, they cannot directly capture the surface of walls, which results in less precise maps where pathways are often missed and the shapes of buildings are all abstracted to rectangles. Even worse, beacon-based estimation does not work indoors, so we need some alternative for more accurate, efficient indoor/outdoor map estimation.

In this paper, we propose a method for simultaneously identifying indoor pathways as well as outer shape and location of the buildings. One crucial design issue is reasonable choice of equipments. As a solution, we employ laser range scanners (LRSs) (or range finders in other words) [4] which can horizontally scan the space (*e.g.*, with a viewing angle of 270°) to detect presence of objects with high precision. Meanwhile, their scan range is limited (the effective range is usually around 20m in most consumer products) compared to wireless beacons which usually travel over 100m. More importantly, LRSs are rather expensive so that not all the team members can be equipped with them. Considering these limitations, the main focus of the proposed method is to achieve faster and more accurate map estimation by simultaneous use of LRSs, wireless beacons and GPS positioning, where the features and precision of their measurement data are quite different. For

978-0-7695-4865-4/12 $26.00 © 2012 IEEE
DOI 10.1109/GreenCom.2012.65

this purpose, we design information fusion approach where the levels of estimation confidence are also estimated within the map estimation process. Since GPS signals are not available indoors, position estimation via Pedestrian Dead Reckoning (PDR) (using accelerometers and digital compasses etc.) is also supported to recognize indoor pathways with LRSs.

Simulation experiments assuming realistic sensor models and field experiments using real laser range scanners have been conducted at several locations of the Osaka University campus. The results have shown that the map estimation was much faster and more precise than the beacon and GPS-based method in the previous work. Also the applicability of the method has been verified by emergency scenarios which have been designed in cooperation with medical doctors in rescue teams.

II. Related Work and Contribution

A. Why does not Robotic SLAM work?

In autonomous robotics, considerable research efforts have been made for Simultaneous Localization and Mapping (SLAM) techniques [5], [6], [7] since recognition of surrounding environment is essential for mobile robots to determine their behavior. They typically employ cameras, range measurement sensors (e.g., laser range scanners) and gyroscopes to create a local map on each robot, and then the entire map of the environment is derived by fusing the local maps of all the robots based on their positions and poses estimated by dead reckoning. The goal of our method is partially similar to these SLAM methods in the sense that it also aims to recognize the surrounding unknown environment. But unfortunately, we can hardly apply the SLAM directly to our case due to the following reason. Unlike robots, we cannot employ a detailed kinematic model for dead reckoning in tracking first responders. A possible alternative is pedestrian dead reckoning (PDR) [8], [9], [10], which has been studied for location-based services in ubiquitous computing. Some literature such as [8], [9] assumes inertial sensors and digital compasses mounted on fixed parts of the user body (e.g., foot, waist, and a helmet). More recently, mobile-phone-based PDR methods [11], [10] have been also investigated to enhance applicability for various ubiquitous services. Despite those highly sophisticated PDR techniques, large error still occurs due to irregular and unpredictable motion of first responders being engaged in rescue activities. Furthermore, unlike robot-based SLAM, it is not realistic to impose additional burdens on those responders to measure the environment. Consequently, measured data obtained from the sensors would be highly unreliable, which also may confuse the mapping process.

B. Mobile Sensor Approach

Xuan et. al. propose indoor map estimation using mobile sensors[12]. They use the 3-axis accelerometers and the 3-axis magnetometers in the smart phone. Also they use the piezometer in a Nike running shoe. This method estimates orientation of buildings and length of wall based on PDR. They should walk along the walls in buildings many time. However, in our case, it is not preferable to impose a limit on the movement of the first responders.

Wireless sensor networks have provided different approaches for detecting the shapes and positions of objects. Wang et. al. [13] presented a method to identify boundary of the sensor network topology, which usually has physical correspondence such as building floor plans. However, such methods require dense deployment of sensor nodes, and thus are not suitable for disaster situations where rapidly grasping overall situation is important.

For reasonable mapping in disaster areas, Minamimoto et. al. have proposed a map generation method using GPS-equipped mobile devices carried by the first responders [2], [3]. Although it quickly builds a coarse-grained map, it does not support indoor mapping since GPS rarely works indoors. Another challenge is that reliability of GPS and wireless communication logs significantly depends on the environment; performance of GPS can be degraded in urban canyons, while wireless signal propagation between the nodes can be affected by multipath effect. Considering such potential error-inducing factors, more adaptive and flexible approach is preferable.

C. Data Fusion Technique

To obtain accurate knowledge from low-cost sensors or unreliable measurement, multiple information fusion techniques have been used in many diverse application areas such as Intelligent Transportation Systems [14], [15], object tracking [10], [16], and activity recognition [17]. The common idea is that combining data from multiple information sources could help complement insufficient data and reduce uncertainty. A basic approach is to employ Bayesian inference that uses probabilities to represent degrees of belief [18]. Then, subjective estimates can be made based on well-known Bayes' rule. It was generalized in Dempster-Shafer theory of evidence, allowing to distribute support for proposition not only to a proposition itself but also to the union of several propositions to handle uncertainty [17]. Artificial neural networks (ANNs) have also been perceived as a powerful and self-adaptive tool, but choosing the most appropriate network topology for the problem is a challenge [15], [16]. Another widely-used approach is summing fusion, where confidence of each proposition is summed so that the one with the highest overall result is adopted [19]. It is very simple and thus suitable for large-scale deployment, so that the decision fusion mechanism of our mapping algorithm basically relies on the idea. To identify appropriate confidence function is a key to ensure reasonable performance with this scheme.

D. Our Contribution

Based on the discussion above, our contribution is two-fold. First, we propose a novel method for instantly creating a precise indoor/outdoor map that seamlessly covers the whole disaster site. For this purpose, we assume that first responders hold GPS-equipped mobile devices during their rescue activity, while some of them wear a special jacket to which an LRS is attached. Combining information from multiple sources (i.e.,

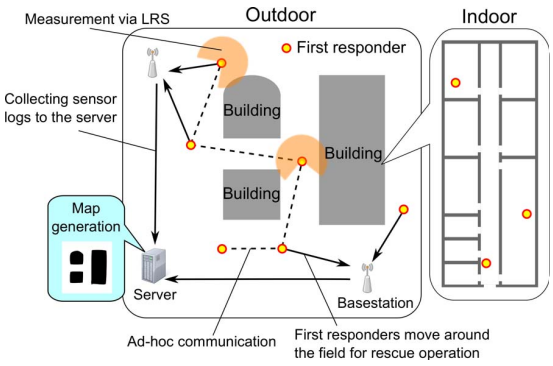

Fig. 1. System Architecture and Operation

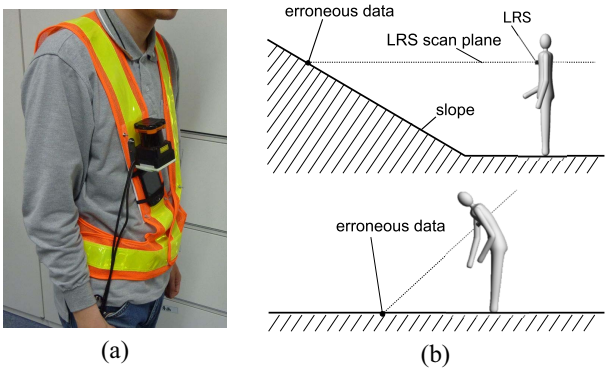

Fig. 2. Attachment of LRS: (a) LRS-equipped Vest (used in experiments), (b)Example of Erroneous Data.

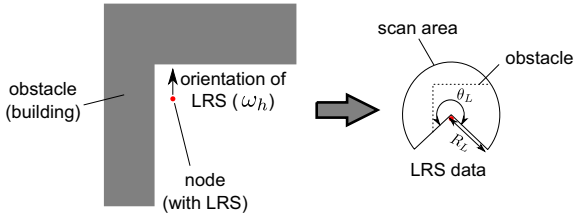

Fig. 3. LRS Scan Area

GPS, PDR, WiFi, and LRSs), it achieves fast and accurate mapping. Our extensive simulations and field experiments show that the use of LRSs enables recognition of indoor pathways and precise outer shape of the buildings, which has yet to be solved in the previous work. We also show that precise information from LRSs greatly helps to accelerate the map generation process. Secondly, we introduce a novel information fusion algorithm, called *adaptive information fusion*. By estimating the confidence of each information sources, it autonomously adapts to various environments (including both indoor and outdoor) to achieve robust mapping.

III. Method Overview

A. System Architecture

Fig. 1 illustrates system architecture and operations. We consider regions that contain buildings and street/pathways between them. Our system consists of a centralized server and a team of mobile nodes (first responders). Each mobile node has a GPS receiver and a wireless communication device with WiFi-level transmission range (*e.g.* at least several tens of meters with clear LoS). The estimated (maximum) transmission range is referred to as R_C. Some of mobile nodes have Laser Range Scanners (denoted as LRSs) with 3D orientation information, which can be obtained by combination of several motion sensors and geomagnetic sensors. Mobile nodes walk for rescue operations, and LRS nodes may enter buildings to scan their inside. As shown in Fig. 2(a), LRSs are attached to LRS holders to scan space horizontally. However, an ideal pose cannot be always maintained, and as illustrated in Fig. 2(b), LRSs may scan the ground and floors rather than walls. Therefore, such noise should be eliminated from the measurement, and we will discuss this issue later.

B. Measurement by Mobile Nodes

All mobile nodes record positions and neighbor measurements and LRS nodes also record wall measurement. The **position measurement** is done by each node's GPS and/or PDR. Nodes without PDR capability (non-LRS nodes) become position-blind inside buildings, and during the time they record the "unknown" state. Nodes identify indoor/outdoor positions by GPS signal availability, and this information is attached to the position measurement. The **neighbor measurement** is done by beacon monitoring. Each node periodically transmits beacons to its neighbors to let them know his/her presence. If node i transmits a beacon with a sequence number at time t, then it records its transmission. If node j receives a beacon from node i at time t, then (i, j) is recorded with the sequence number as a successful beacon transmission event from i to j. Finally, the **wall measurement** is done by LRS. Each LRS-node continuously scans space by LRS, and the space is represented as a fan-shaped 2D area with radius R_L and angle θ_L. By using LRS, the distance to the closest object in each angle in $[-\theta_L/2,\ \theta_L/2]$ with step interval $\Delta\theta_L$ is obtained where angle 0 represents the LRS orientation ω_h as shown in Fig. 3.

C. Collection of Measurements

Measurements by mobile nodes are uploaded to a single server, via 3G cellular or other broadband technologies. Alternatively, we may set a portable server (like a laptop) and WiFi base stations at the site for more severe conditions where broadband networks and servers die or are not available. We assume that the timeline is divided into time windows of length Δt. We may choose appropriate length as Δt considering GPS, beacon, and LRS measurement intervals.

From position measurements, we generate *position logs* for each pair of time window k and node i (each log is denoted by P_i^k). P_i^k is either the estimated coordinate (or "unknown") with an indoor or outdoor flag. If there is no measurement during the time window, we may fill the gap by interpolation or some other techniques. From the neighbor measurement and the above position logs, we generate *communication logs* for each pair of time window k and node i (each log is denoted by C_i^k). C_i^k contains a set of neighbors within the maximum transmission range R_C and indicates whether

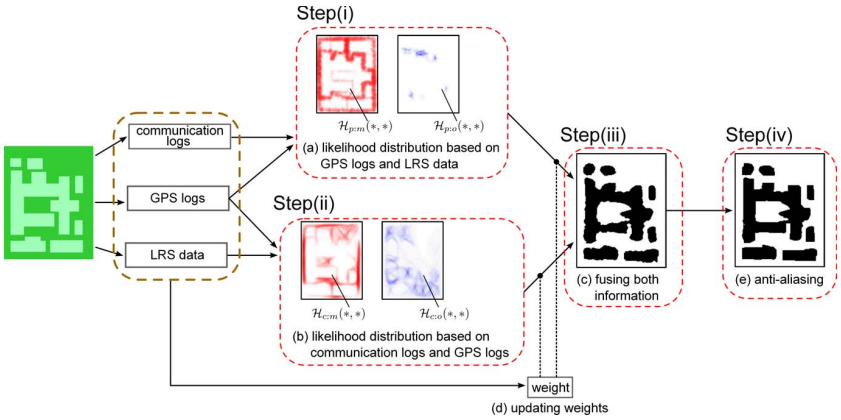

Fig. 4. Map Generation Process

those neighbors could receive node i's beacon(s) transmitted during time window k or not. For example, assume node i transmitted a beacon at position P_i^k and nodes u, v and w are those neighbors within R_C from P_i^k. If only u and v could hear the beacon, then $C_i^k = \{u, v, \overline{w}\}$ indicating that w could not receive the beacon even though w was in the expected transmission range. Finally, from the wall measurement by LRS and the above position logs, we generate *LRS logs* for each pair of time window k and node i (each log is denoted by L_i^k). LRS mounted on human may detect different objects according to their pose and environment (such as ground/floor surface detection shown in Fig. 2(b)). We eliminate such measurement that scans with deviated vertical orientation to eliminate such errors. Additionally, long scan range may increase errors since the number of laser beams on the object surface decreases as distance increases. Therefore, although consumer-level LRSs usually have 20m or longer ranges[4], we limit the range around 10m (*i.e.* we set $R_L = 10m$). By the above, we finally obtain L_i^k that consists of distance information for each (absolute) orientation θ_h ($h \in [\lceil(\omega_h - \theta_L/2)/\Delta\theta_L\rceil, \lceil(\omega_h + \theta_L/2)/\Delta\theta_L\rceil]$).

In summary, for each time window k and node i, we have P_i^k, C_i^k and L_i^k as position, communication and LRS logs, respectively (some logs may be empty).

D. Map Generation Algorithm Overview

Initially, we have a white map that has been divided into square cells of the same size. We refer to (x-th, y-th) cell as $c(x, y)$.

Six non-negative likelihood values are associated with each cell. $\mathcal{H}_{p:o}(x, y)$ and $\mathcal{H}_{p:m}(x, y)$, determined by position and LRS logs, denote the likelihood values that $c(x, y)$ are in obstacle area and movable area, respectively. Similarly, $\mathcal{H}_{c:o}(x, y)$ and $\mathcal{H}_{c:m}(x, y)$, determined by position and communication logs, denote the likelihood values that $c(x, y)$ are in obstacle area and movable area, respectively. These values are for outdoor map generation. For indoor cases, we introduce $\tilde{\mathcal{H}}_{p:o}(x, y)$ and $\tilde{\mathcal{H}}_{p:m}(x, y)$ that correspond to $\mathcal{H}_{p:o}(x, y)$ and $\mathcal{H}_{p:m}(x, y)$, respectively. Both indoor and outdoor map generation is performed simultaneously, according to the indoor/outdoor flags of position logs.

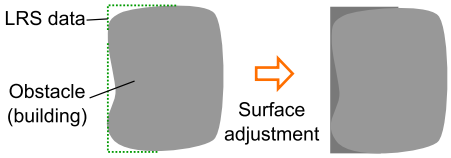

Fig. 5. Surface Adjustment by LRS measurement

The outline of outdoor map generation is illustrated in Fig. 4. **(i) Likelihood Estimation from Position and LRS logs.** Since position and LRS logs indicate movable area and obstacles around nodes, we update $\mathcal{H}_{p:o}(x, y)$ and $\mathcal{H}_{p:m}(x, y)$. Fig. 4(a) visualizes these likelihood values where white mean 0 likelihood values. **(ii) Likelihood Estimation from Position and Communication Logs.** We also update $\mathcal{H}_{c:o}(x, y)$ and $\mathcal{H}_{c:m}(x, y)$ by communication logs and position logs. We assume beacon reception by node j from node i is successful only if they are within R_C distance with a clear line of sight. Therefore, cells between two positions with successful beacon transmission are likely to be movable cells, and to be obstacle cells otherwise. Fig. 4(b) visualizes these likelihood values. **(iii) Map Generation from Likelihood.** When we need to obtain a map, we combine the likelihood for each cell. The weights in combining these values are determined online, by analyzing the three logs (Fig. 4(c)). The weights are adaptively updated (Fig. 4(d)) as logs are accumulated. **(iv) Anti-Aliasing using LRS logs.** LRS logs that are expected to improve the surface estimation are used for such a purpose as illustrated in Fig. 5.

For indoor cases, communication logs are not reliable since indoor wireless propagation is much more complex. Therefore, we skip step (ii) in indoor cases. Also the position logs are generated by PDR, which has different characteristics of errors. Therefore, we provide a different algorithm for indoor cases.

The weights should appropriately be determined based on their confidence levels of three types of logs. The confidence levels are dependent on LRS node and non-LRS node density, node mobility, scan and communication ranges and many other factors. For example, if we have more LRS nodes, the amount

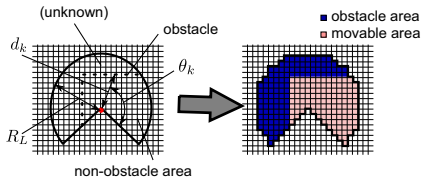

Fig. 6. Obstacle Estimation by LRS Logs

of LRS logs may increase, and $\mathcal{H}_{p:o}(x,y)$ and $\mathcal{H}_{p:m}(x,y)$ should be weighted more than $\mathcal{H}_{c:o}(x,y)$ and $\mathcal{H}_{c:m}(x,y)$ (LRS-based estimation is considered more reliable). Therefore, we try to maximize the confidence of the mixed likelihood. For this purpose, we automatically determine the best set of weights in our map estimation process.

IV. Design Details

We describe the design details in the following subsections.

A. Likelihood Estimation from Position and LRS logs

Recall each LRS log L_i^k of node i at time window k is a set of distance data d_h for θ_h ($h \in [\lceil(\omega_h - \theta_L/2)/\Delta\theta_L\rceil, \lceil(\omega_h + \theta_L/2)/\Delta\theta_L\rceil]$), and the distance shorter than R_L indicates an obstacle in the orientation. Although we cannot know the thickness of the obstacles by LRS scan, building sizes are usually ten meters or more and cells beyond the surface are likely to be obstacle cells. This may be a wrong estimation, but such erroneous data are expected to be eliminated as many logs are applied. Fig. 6 illustrates this process. From cell P_i^k, all the cells to orientation θ_h with distance over d_h up to R_L are regarded as obstacle cells. Furthermore, trajectory between two subsequent positions P_i^k and P_i^{k+1} consists of movable cells. For simplicity, the trajectory is approximated by a line segment and these cells on the line are regarded as movable cells.

We consider the effect of position errors in updating likelihood values of cells. In this paper, we assume that distance errors of GPS follow normal distribution $\mathcal{N}(0,\sigma_g^2)$ and directional errors are uniform. We let f_g denote the probability distribution function of GPS distance error for relative coordinates $(\Delta x, \Delta y)$ from the true coordinates. If cell $c(x,y)$ is regarded as an obstacle cell (or movable cell), for each cell $c(x+\Delta x, y+\Delta y)$ we add the following value $e(\Delta x,\Delta y)$ to the likelihood value $\mathcal{H}_{p:o}(x+\Delta x, y+\Delta y)$ (or $\mathcal{H}_{p:m}(x+\Delta x, y+\Delta y)$) if P_i^k is outdoor, and add the same value to the likelihood value $\tilde{\mathcal{H}}_{p:o}(x+\Delta x, y+\Delta y)$ (or $\tilde{\mathcal{H}}_{p:m}(x+\Delta x, y+\Delta y)$) if P_i^k is indoor where S denotes the cell length.

$$e(\Delta x,\Delta y) = \int_{-\frac{S}{2}}^{\frac{S}{2}}\int_{-\frac{S}{2}}^{\frac{S}{2}} f_g(u+S\Delta x, v+S\Delta y)dudv \quad (1)$$

In the normal distribution, almost all (99.74%) of the values are within the range $\pm 3\sigma_g$. Therefore we update those cells within distance $3\sigma_g$ from $c(x,y)$. As for PDR, we may follow the PDR error model in literature (such as our indoor localization [11]), but they assume mobility without mobility restrictions. Meanwhile, we focus on restricted mobility in indoor cases where mobile nodes move on corridor or hallways to find movable pathways in rescue operation. Also in indoor cases, LRS measurement is much more stable than outdoor cases since floors are flat and hallways are narrow (easy to track continuous walls). Considering these facts, we approximate PDR by straight lines unless a sudden change of orientation is detected. After the orientation changes, we restart approximating PDR by a new line. Therefore, we have directional errors for each line and add likelihood values in a similar way as the above GPS case.

Formally, $\mathcal{H}_{p:o}(x,y)$ and $\mathcal{H}_{p:m}(x,y)$ are calculated and updated as position and LRS logs are updated. At time window 0, $\mathcal{H}_{p:o}(x,y)$ and $\mathcal{H}_{p:o}(x,y)$ are set to zero. (1) For each pair of P_i^k and $\theta_h \in L_i^k$, label the cells on this radial line (length R_L) within distance d_h from P_i^k with "movable" and label the cells between d_h and R_L with "obstacle". Also label all those cells with the indoor/outdoor flag of P_i^k. (2) For each pair of P_i^{k-1} and P_i^k, label the cells between them with "movable". Also label all those cells with the indoor/outdoor flag of P_i^k. (3) For each cell $c(x,y)$ labeled with "obstacle" and "outdoor", add $e(\Delta x,\Delta y)$ of Eq. (1) to $\mathcal{H}_{p:o}(x+\Delta x, y+\Delta y)$. (4) For each cell $c(x,y)$ labeled with "movable" and "outdoor", add $e(\Delta x,\Delta y)$ of Eq. (1) to $\mathcal{H}_{p:m}(x+\Delta x, y+\Delta y)$. We omit the indoor cases since the process itself is essentially the same.

B. Likelihood Estimation from Position and Communication Logs

We introduce a simple likelihood estimation method by communication logs. No obstacle is assumed between two positions with successful beacon transmission, and the presence of obstacle between them with transmission failure. This is not always true since the real world wireless propagation is hard to predict. For example, diffraction and reflection by building walls may happen in building canyon, which may result in unexpected success of communication beyond obstacles. Also transmission failure may occur by other reasons such as interference. We consider that these phenomena that cause estimation errors are more likely to occur as two nodes are more distant. Thus we introduce the following parameter that reduces the likelihood to be added to "obstacle" cells

$$p(d) = 1 - \frac{d}{R_C} \quad (2)$$

where d is the distance between nodes.

Similarly with the previous section, GPS errors should be considered. We use the same $e(\Delta x,\Delta y)$ in Eq. (1). In case of obstacle cells, we use $e(\Delta x,\Delta y)$ multiplied by $p(d)$ to add the reduced likelihood value to cell $c(x+\Delta x, y+\Delta y)$.

Formally, $\mathcal{H}_{c:o}(x,y)$ and $\mathcal{H}_{c:m}(x,y)$ are updated as follows. These values are initially set to zero. (1) Label cells on the line segment between node i and node j with "movable" if $j \in C_i^k$. (2) For each cell $c(x,y)$ labeled with "movable", add $e(\Delta x,\Delta y)$ to $\mathcal{H}_{c:m}(x+\Delta x, y+\Delta y)$. (3) Label cells on the line segment between node i and node j with "obstacle" if $\overline{j} \in C_i^k$. (4) For each cell $c(x,y)$ labeled with "obstacle", add $p(d)\cdot e(\Delta x,\Delta y)$ to $\mathcal{H}_{c:m}(x+\Delta x, y+\Delta y)$ where d is the Euclid distance between i and j.

C. Map Generation from Likelihood Values

An outdoor map is obtained by the four likelihood values $\mathcal{H}_{p:o}(x,y)$, $\mathcal{H}_{p:m}(x,y)$, $\mathcal{H}_{c:o}(x,y)$ and $\mathcal{H}_{c:m}(x,y)$ for each $c(x,y)$. Since they are independently updated, and since confidence levels of these information sources are different depending on scenarios and environments, we design an adaptive algorithm to determine the weights (coefficients) in linear combination. We introduce the following weighted linear function of the likelihood values to determine an outdoor obstacle map.

$$\begin{aligned}\mathcal{M}_{obs}(x,y) &= w_{p:o}\mathcal{H}_{p:o}(x,y) - w_{p:m}\mathcal{H}_{p:m}(x,y) \\ &\quad + w_{c:o}\mathcal{H}_{c:o}(x,y) - w_{c:m}\mathcal{H}_{c:m}(x,y) \quad (3)\end{aligned}$$

Then $c(x,y)$ is determined as obstacle cell if the above value is not less than the *outdoor obstacle boundary threshold* α, and movable cell otherwise. Similarly, we introduce the following likelihood value for indoor cases, and use the *indoor obstacle boundary threshold* $\tilde{\alpha}$ to determine if $c(x,y)$ is obstacle or movable.

$$\tilde{\mathcal{M}}_{obs}(x,y) = \tilde{w}_{p:o}\tilde{\mathcal{H}}_{p:o}(x,y) - \tilde{w}_{p:m}\tilde{\mathcal{H}}_{p:m}(x,y) \quad (4)$$

As we discussed earlier, these likelihood values are dependent on node mobility and density, GPS positioning errors and other various factors. Therefore, according to the estimation of their confidence levels, $w_{p:o}$, $w_{p:m}$, $\tilde{w}_{p:o}$, $\tilde{w}_{p:m}$, $w_{c:o}$ and $w_{c:m}$ are determined online, rather than using fixed values.

The following is the algorithm to determine these weights. We define W^k as a set $\{w_{p:o}, w_{p:m}, w_{c:o}, w_{c:m}, \alpha\}$ of weights and threshold at time window k. We also denote the sets $\bigcup_{i\in N} L_i^k$, $\bigcup_{i\in N} P_i^k$ and $\bigcup_{i\in N} C_i^k$ of logs at time k as L^k, P^k and C^k, respectively, and the time-collective sets $\bigcup_{z\in 1..k} L^z$, $\bigcup_{z\in 1..k} P^z$ and $\bigcup_{z\in 1..k} C^z$ as $\mathbf{L^k}$, $\mathbf{P^k}$ and $\mathbf{C^k}$, respectively. At time window k, the probability that W^k is optimal under given logs $\mathbf{L^k}$, $\mathbf{C^k}$ and $\mathbf{P^k}$ is represented as a posterior probability $P(W^k|\mathbf{L^k},\mathbf{C^k},\mathbf{P^k})$. We use W^k that maximizes this probability at time window k as the optimal weight set. Assuming that measurements at different time windows are independent, the following equation is derived according to the Bayes' theorem where η is an coefficient for probability normalization.

$$\begin{aligned}&P(W^k|\mathbf{L^k},\mathbf{C^k},\mathbf{P^k}) \\ &= \eta P(L^k,C^k,P^k|W^k)\cdot P(W^k|\mathbf{L^{k-1}},\mathbf{C^{k-1}},\mathbf{P^{k-1}}) \\ &= \eta P(L^k,C^k,P^k|W^k) \\ &\quad \cdot\int P(W^k|W^{k-1})\cdot P(W^{k-1}|\mathbf{L^{k-1}},\mathbf{C^{k-1}},\mathbf{P^{k-1}})dW^{k-1} \quad (5)\end{aligned}$$

This indicates that by determining $P(L^k,C^k,P^k|W^k)$ and $P(W^k|W^{k-1})$ properly, $P(W^k|\mathbf{L^k},\mathbf{C^k},\mathbf{P^k})$ can be determined using the probability $P(W^{k-1}|\mathbf{L^{k-1}},\mathbf{C^{k-1}},\mathbf{P^{k-1}})$ of time window $k-1$.

Then we address how to determine the values of $P(L^k,C^k,P^k|W^k)$ and $P(W^k|W^{k-1})$. Since the amount of measurements gradually increases as time passes, W^k should take similar values with W^{k-1}. Therefore, as $P(W^k|W^{k-1})$, we may employ a monotonically decreasing distribution where mean 0 takes the maximum probability, such as a normal distribution with mean 0. On the other hand, $P(L^k,C^k,P^k|W^k)$ is a probability of obtaining logs L^k, C^k and P^k for given W^k. Since L^k and C^k are fully independent, we may derive $P(L^k,P^k|W^k)$ and $P(C^k,P^k|W^k)$ independently and let their average be the value of $P(L^k,C^k,P^k|W^k)$.

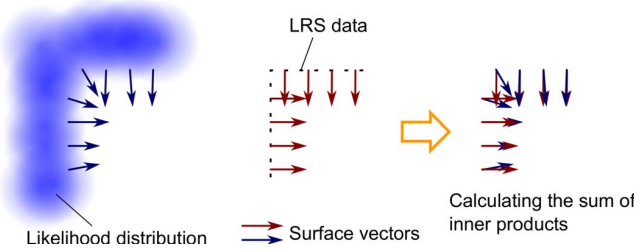

Fig. 7. Surface Comparison between LRS logs and Obstacle Maps

$P(L^k,P^k|W^k)$ takes higher probability as the likelihood $\mathcal{M}_{obs}(x,y)$ by W^k and logs L^k and P^k are more consistent. In order to quantify the consistency between $\mathcal{M}_{obs}(x,y)$ and L^k, we introduce a set of vectors to represent the characteristics of the (estimated) surface of obstacles in the obstacle map ($\bigcup_{x,y}\mathcal{M}_{obs}(x,y)$) and each LRS log L_i^k. Those vectors (called normal vectors) are orthogonal to the surface of objects and have different magnitudes. Normal vectors in LRS logs can be derived in a usual way by estimating the surface from adjacent scanned points. On the other hand, we have to consider the likelihood values in the obstacle map. We set a larger magnitude of normal vector as likelihood $\mathcal{M}_{obs}(x,y)$ is close to the boundary threshold α or $\mathcal{M}_{obs}(x,y)$ is more different than its neighboring cells (has a larger gradient). To represent the above, we multiply a decreasing function of the difference of likelihood and α with the gradient to determine the magnitude of normal vectors.

As illustrated in Fig. 7, we obtain the probability $P(L^k,P^k|W^k)$ by W^k and LRS logs L^k. Then for pair of vectors of $\mathcal{M}_{obs}(x,y)$ and of L^k at the same position, we take their inner product, and transform the value of $P(L^k,P^k|W^k)$ into the range [0,1] using non-decreasing function such as a Sigmoid function.

Similarly, $P(C^k,P^k|W^k)$ takes higher probability as likelihood $\mathcal{M}_{obs}(x,y)$ by W^k and logs C^k and P^k are more consistent. In particular, there are most consistent as the obstacle likelihood values of cells between two points with successful beacon transmission are smaller, and as they are larger for transmission failure. Therefore, we introduce the following metric $L_{NP} = \eta_N L_N - \eta_P L_P$ where L_N and L_P are the sums of the maximum likelihood values in each communication failure case, and of those in each communication success case, respectively (η_N and η_P are coefficient to normalize those values). We translate the value of L_{NP} into the range [0,1] by a non-decreasing function and use it as $P(C^k,P^k|W^k)$.

Finally, for indoor cases, we consider $\tilde{W}^k = \{\tilde{w}_{p:o}, \tilde{w}_{p:m}, \tilde{\alpha}\}$ instead of W^k since we do not use communication logs. The posterior probability $P(\tilde{W}^k|\mathbf{L^k},\mathbf{P^k})$ is determined as follows (P^k is obtained by PDR).

$$P(\tilde{W}^k|\mathbf{L^k},\mathbf{P^k}) = \eta P(L^k,P^k|\tilde{W}^k) \cdot\int P(\tilde{W}^k|\tilde{W}^{k-1})P(\tilde{W}^{k-1}|\mathbf{L^{k-1}},\mathbf{P^{k-1}})d\tilde{W}^{k-1} \quad (6)$$

D. Anti-aliasing of Surface using LRS logs

At this moment, we have determined the obstacles and their surface. To eliminate irregularity, we finally apply LRS logs to reproduce the precise wall measurement. For this purpose, LRS log placement on the obstacle map is performed by seeking the corresponding surface in the obstacle map. We take the same approach as we described in Section IV-C to quantify the consistency of obstacle map and LRS logs. For each candidate location q_k, we define $P(L^k|W^k,q_k)$ which is determined by the inner product of their normal vectors. Then it is multiplied by position distance and directional error probability distribution functions, and LRS log placement is performed if the value exceeds a certain threshold. As for the position error model, we use the same model as introduced in Section IV-A and as for the directional error model we assume a normal distribution.

V. Simulation

A. Simulation Settings

We evaluated the performance of our method through several simulations using the network simulator QualNet [20]. In the simulations, we employed two target fields each of which models the office buildings of the Engineering Science Department (Fig. 8 (a)) and Health Science Department (Fig. 8 (b)) of the Osaka University, respectively. The fields consist of the area of 10,000 m^2 to 30,000 m^2, including both obstacle areas (i.e., buildings and the regions that cannot be entered by first responders) and movable areas. The number, density and shapes of the buildings are different for each case. Nodes are assumed to move along the paths indicated by the lines in Fig. 8 and randomly choose their direction at each intersection. To compare the performance with previous method[2], [3] that supports only outdoor situations, all the nodes move outdoors in this scenario. The nodes are initially placed on the movable paths at random, and then move at a speed that follows a Gaussian distribution with a mean of 1.5 m/sec and a standard deviation of 0.01. If LRS is available, the node acquires range information within a fan-shaped region centered at its current location and orientation. The maximum detectable range and viewing angle of the LRS are set to $R_L = 10$m and $\theta_L = 270°$, respectively. Since range measurement error of LRS is much smaller than GPS errors, it is negligible and not taken into account in this evaluation. Also, we do not discard any LRS logs, assuming that LRS can keep horizontal position while normal walking motion. Wireless communication between the nodes are simulated using Wireless Insite extension [21] of the QualNet, which is capable of realistic simulations of radio propagation based on detailed 3D models of the environment. 2.4GHz ISM band is used for the wireless communications, while transmission power is determined so that the maximum

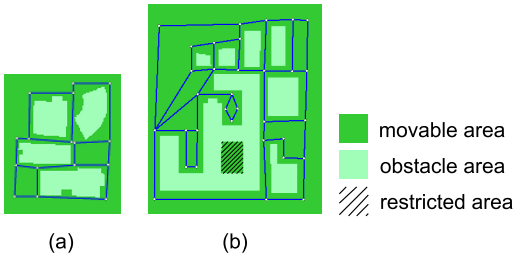

Fig. 8. Field Maps (Simulation)

communication range is 50m with the two-ray ground reflection model [22]. IEEE 802.11b is used for the wireless communication protocol. The current location of the node is obtained via GPS every second, where GPS errors follow a zero-mean Gaussian distribution with a standard deviation of 5 m. The parameters related to map generation are as follows. We set the cell size to 1m $\times$ 1m and assume that the maximum communication range $R = 50$m. In calculating likelihood, we set the standard deviation of the distribution as $\sigma_g = \sqrt{3}$m. Unless otherwise noted, we assume $N = 15$ and $N_L = 5$, where N is the number of nodes and N_L of them are equipped with LRS.

Our method assumes the use in rescue operations. In these case energy consumption is not so big problem, because operation time is at most around several hours. Precision, perceptibility and the estimation time is more important.

So, in the above settings, we ran a simulation for 600 seconds and evaluated *cell recognition rate* (CRR) and *path recognition rate* of the generated map. The former metric is defined by the rate of the number of cells that are correctly identified whether it is a movable area or an obstacle area. The latter is defined by the rate of the number of paths that are not incorrectly obstructed in the map. The simulation results will be given in the next section.

B. Simulation Results

1) Basic Performance: In Fig. 9, we compare the performance of our method to the previous method [2], [3] (without LRS) in terms of cell recognition rate for the field (b). For both methods, we can see that the cell recognition rate steeply grows at the beginning and then converges at a certain level. The proposed method could achieve the cell recognition rate of 90% in 200 seconds, while the previous method took 400 seconds to reach the accuracy of 80%. In our setting which is 15 node randomly choosing their paths, the time from 200 seconds to 300 seconds is necessary so that each path is visited at least once. Because our method achieves high accuracy in that time, it is a very efficient method in contrast to previous method. This improvement would mainly come from the use of LRS. Since it provides precise shape of the buildings and their distance, a more accurate map could be built with less sensor logs. Remember that we let only five nodes out of 15 carry LRSs in this simulation. The result shows that we can significantly accelerate and refine the map generation if a small number of nodes hold LRSs.

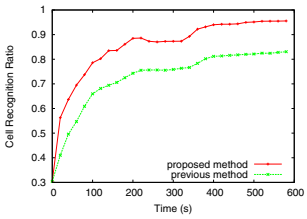

Fig. 9. Cell Recognition Rate

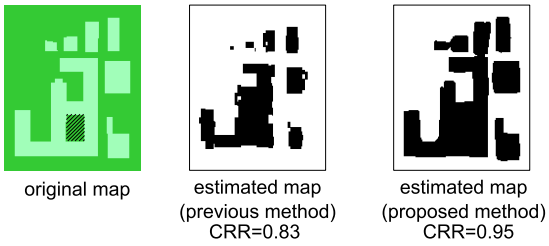

Fig. 10. Comparison of Generated Maps

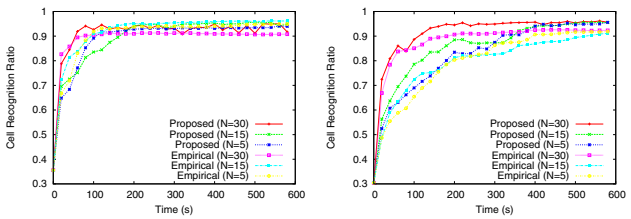

(a) (b)

Fig. 11. Contribution of Adaptive Information Fusion: figures (a) and (b) show the cell recognition rates for the fields (a) and (b) in Fig.8, respectively.

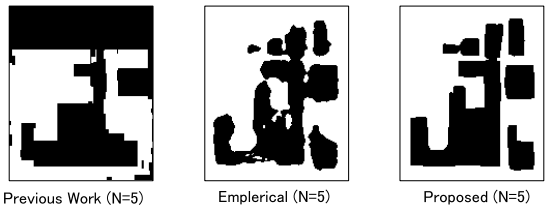

Fig. 12. Contribution of Adaptive Information Fusion (Generated Maps)

Regarding path recognition capability, we got a high path recognition rate of 98%. Since finding movable paths is essential for first responders to build their strategy for rescue operations, it would be a desirable feature to achieve our goal.

The estimated maps produced by the both methods are shown in Fig. 10. We can see that improving the cell recognition rate from 80% to 90% really affects the perceptibility of the resulting maps. The proposed method could reflect the original map more faithfully.

2) Effectiveness of Adaptive Information Fusion: To show the effectiveness of our adaptive information fusion mechanism, we also compared the performance of our method to the case that constant weights are used in the final map fusion. In the compared method, say *Empirical*, the weights are determined by the following strategy: "Obstacle" decision based on communication logs is less credible than other cases since all the cells between two nodes that cannot communicate with each other are regarded as obstacle cells even though most of them may be actually non-obstacle ones. Hence, we decided to assign less value for $w_{c:o}$ than $w_{p:o}$, $w_{p:m}$, and $w_{p:m}$. In addition, after extensive simulations with various patterns of target fields, we found that a simple assumption of $w_{p:o} = w_{p:m} = w_{c:m} = 1$ gives relatively good results for most outdoor cases. Based on the observations above, we derived an empirical formula that identifies the best $w_{c:o}$ using average likelihood values and the standard deviation of GPS errors.

Fig. 11 shows the cell recognition rate for each case with different node densities, namely $N = 5, 15, 30$. For most N, cell recognition rate of the adaptive approach is higher than that of *Empirical* almost throughout the experiment.

Next, we confirm how our adaptive information fusion algorithm adjusts the confident level of each information source. Table I lists the final weight values after running a simulation for 600 seconds; we can see that different weights are assigned according to the types of target fields and node densities. When the node density is low, each node can find fewer neighbors within its communication range, and thus less communication logs can be collected. Also, reliability of measurement data from GPS, LRSs, and wireless beaconing depends on arrangement of buildings, geometrical features and node mobility, as we have described in the previous sections. The results show that our algorithm could adopt to the such different features of collected information.

In Fig. 12, we show the estimated maps by *Empirical* and our adaptive approach as $N = 5$. As seen, the proposed method could reflect the shape of the building much more accurately, since appropriate weights are assigned according to the environment. In this figure, we also compare the resulting maps with that of the previous work. For the previous method with $N = 5$, the cells in the movable area at the top of the field are misidentified as obstacle cells. This is because few nodes passed through the region during the experiment time, and thus it could not collect sufficient amount of GPS and communication logs. In contrast, the proposed method could generate a complete map under the same conditions, since LRSs could complement the insufficient measurement data.

3) Impact of Node Density: In Fig. 11, we can also see that the accuracy converges more quickly as N is larger. It is natural since a large amount of GPS and communication logs can be collected when many nodes participate in the map generation, which means the logs can fastly cover all over the field. After sufficient time has elapsed, the cell recognition rate converges to the similar value for every case since the "coverage" of LRS logs gets higher.

4) Contribution of LRS Logs to the Perceptibility: Fig. 13 shows the effect of our surface adjustment algorithm. In the map (a), we can see that the corners of each building are rounded due to uncertainty near the boundaries. In contrast, the correct shape of the buildings are reflected in the map (b) after applying the surface adjustment process based on LRS logs; even a concavity of the building (at the bottom) can be clearly seen in the map. Thus, our adjustment mechanism

TABLE I
ADJUSTED WEIGHTS FOR INFOMATION FUSION

	N	$w_{p:o}$	$w_{p:m}$	$w_{c:o}$	$w_{c:m}$	α
field (a)	5	2.0	2.0	7.0	7.0	-0.02
	15	3.0	3.0	5.0	3.0	-0.02
	30	3.0	3.0	7.0	3.0	-0.02
field (b)	5	3.0	3.0	7.0	7.0	-0.02
	15	3.0	3.0	5.0	3.0	-0.02
	30	5.0	5.0	5.0	3.0	-0.02

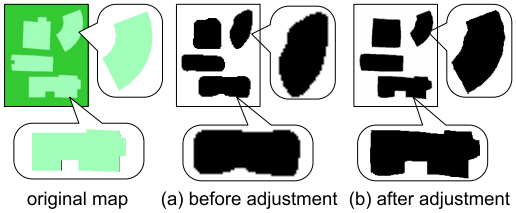

Fig. 13. Efficacy of Surface Adjustment

successfully enhances the perceptibility of the estimated maps.

5) Performance in Emergency Scenario: In previous section, we assume that nodes randomly choose their directions. In this section, we use the mobility which models realistic rescue operations. Usually, if there are many injured people, first responders set up the emergency relief place, and they perform search and conveyance of the injured people.We model such activities by two types of nodes. The first type is called "exploration node" which moves around the entire region to search injured people and grasp the spot. Another type is called "conveyance node" which commutes between the relief place and any point in the region to convey injured people. We perform the simulation using field (a) and we assume that left lower intersection is the relief place. Exploration nodes start from the relief place and visit all paths in the region. Conveyance nodes commute between the relief place and other intersections which are randomly selected whenever they come back to the relief place. We set $N = 15$ and $N_L = 5$. The number of exploration nodes is 10 and the number of conveyance nodes is 5.

Fig.14 shows the cell recognition rate for each case in which exploration nodes have LRSs or conveyance nodes have LRSs. As a result of using this mobility, the cell recognition rate could reach the same level as using random path choosing mobility. Furthermore, convergence of the cell recognition rate is quick, because exploration nodes go around the entire region efficiently.

VI. EVALUATION WITH REAL LRS LOGS

A. Evaluation Methodology

In the previous section, we employed the Wireless Insight module to generate communication logs in a realistic fashion. On the other hand, we assumed a simple measurement model for LRS where ranging errors and the effect of its slight vibration due to walking motion are not taken into account. To confirm the performance in more realistic environment and validate the assumptions in our simulations, we also tried

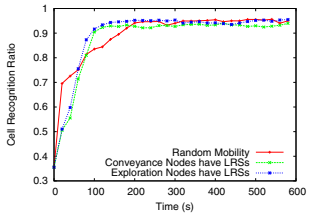

Fig. 14. Performance in emergency scenario

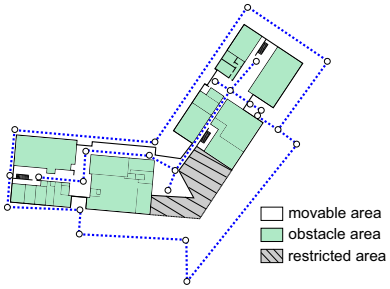

Fig. 15. Field map (IST Dept.)

generating a map using real LRS logs. In this experiment, we consider both indoor and outdoor cases to show how they collaborate with.

The sensor logs were collected through the following experiment being conducted around the office buildings of Information Science and Technology Department. The field map is shown in Fig. 15, where the movable paths are overlaid. Note that the paths go through not only outdoor but also indoor areas. In the same way as the previous section, node mobility patterns were randomly generated along the paths. Following the generated random mobility patterns, an examinee walked around the field with an LRS for 600 seconds. While the experiment, a Hokuyo UTM-30LX Laser [4] was attached to his jacket as shown in Fig. 2. Although it has the maximum detectable range of 30m, we discarded range measurement logs that exceeds 10m due to the limitation on the pose estimation accuracy of LRS (given by inertial sensors). After conducting such experiments 3 times, we collected three sequences of real LRS data.

Using the real sensor logs, we ran simulation with similar settings as those in Section V. Here, we set $N = 10$ and $N_L = 3$, and applied the collected range measurement logs to the three LRS-equipped nodes. Since we can correct PDR traces by matching them with LRS logs, we assume that the PDR error follows a zero-mean Gaussian distribution with a standard deviation of 0.2m. Other simulation settings are the same as those of Section V.

B. Results

The outer shape of the buildings is estimated by the logs from the nodes outdoors, while passages inside the building are identified using those indoors. Then, the two maps are merged into a seamless indoor/outdoor map as shown in Fig. 16. We can see that both outer shape of the building and passages indoors are successfully reflected to the final map.

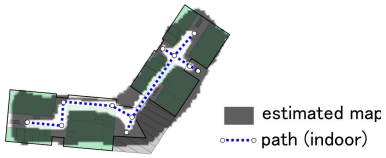

Fig. 16. Generated Map (Overlaid)

In general, indoor passages are much narrower than roads and pathways outdoors, and thus hard to be detected. LRSs are really suitable for such situations; they provide more reliable measurements indoors since the floor is usually flat within a building. A challenge is to handle the large variance in the features of collected sensor logs according to the situations. GPS logs cannot be obtained indoors, while LRS logs might be deteriorated outdoors due to ups and downs of the field. Also, wireless communication logs can be highly affected by multipath effect. The result shows that our adaptive information fusion mechanism copes with this problem and enables a sufficient mapping accuracy and path recognition capability in both indoor and outdoor.

VII. Conclusion

In this paper, we have proposed a novel map estimation method to support rescue operations by first responders. Combining information from multiple sources (*i.e.*, GPS, PDR, WiFi, and LRSs) with different confident levels, it quickly generates an accurate map of the whole disaster site. Our simulation results show that the proposed method could generate a map of a 140m $\times$ 170m field in 200 seconds with accuracy of 90%, while the previous work took 400 seconds to achieve accuracy of 80%. We have also showed that our adaptive information fusion approach helps to enhance mapping precision by autonomously adjusting confident levels of the information sources according to situations. Finally, we have conducted a simulation based on real sensor data collected through a field experiment, and confirmed that our method could successfully reflect the outer shape of the building as well as indoor pathways to the generated map.

For part of our future work, we plan to further refine our algorithms to enhance precision and perceptibility of generated maps by analyzing sensing errors in more detail. Also, we are seeking effective collaboration with other situation-awareness technology such as noxious-gas detection and estimation of pedestrian flows. Overlaying the precise estimated map with such environmental information could greatly support efficient rescue activities.

Acknowledgment

This work was supported by CPS-IP Project (Integrated Platforms for Cyber-Physical Systems to Accelerate Implementation of Efficient Social Systems (FY2012 - FY2016)) in the research promotion program for national level challenges ”research and development for the realization of next-generation IT platforms” by the Ministry of Education, Culture, Sports, Science and Technology (MEXT) and also supported by KDDI Foundation Research Grant Program.

References

[1] T. Higashino, *Advanced wireless communication technology for efficient rescue operations*, Japan Science and Technology Agency. [Online]. Available: http://www.jst.go.jp/kisoken/crest/en/area02/1-04.html

[2] S. Minamimoto, S. Fujii, H. Yamaguchi, and T. Higashino, “Local map generation using position and communication history of mobile nodes,” in *Proceedings of the 8th IEEE International Conference on Pervasive Computing and Communications (PerCom ’10)*, 2010, pp. 2–10.

[3] ——, “Map estimation using GPS-equipped mobile wireless nodes,” *Pervasive and Mobile Computing*, vol. 6, no. 6, pp. 623–641, 2010.

[4] *UTM-30LX*, Hokuyo Automatic Co. LTD. [Online]. Available: http://www.hokuyo-aut.jp/02sensor/07scanner/utm_30lx.html

[5] H. Choset and K. Nagatani, “Topological simultaneous localization and mapping (SLAM) : Toward exact localization without explicit localization,” *IEEE Trans. Robotics and Automation*, vol. 17, no. 2, pp. 125–137, 2001.

[6] H. Durrant-Whyte and T. Bailey, “Simultaneous localization and mapping: PartI,” *IEEE Robotics and Automation Magazine*, vol. 13, no. 2, pp. 99–110, 2006.

[7] A. Howard, “Multi-robot simultaneous localization and mapping using particle filters,” *International Journal of Robotics Research*, vol. 25, no. 12, pp. 1243–1256, 2006.

[8] S. Beauregard, “A helmet-mounted pedestrian dead reckoning system,” in *Proceedings of the 3rd International Forum on Applied Wearable Computing (IFAWC ’06)*, 2006, pp. 1–11.

[9] L. Fang, P. J. Antsaklis, L. A. Montestruque, M. B. McMickell, M. Lemmon, Y. Sun, H. Fang, I. Koutroulis, M. Haenggi, M. Xie, and X. Xie, “Design of a wireless assisted pedestrian dead reckoning system - the NavMote experience,” *IEEE Transactions on Instrumentation and Measurement*, vol. 54, no. 6, pp. 2342–2358, 2005.

[10] Y. Jin, H.-S. Toh, W.-S. Soh, and W.-C. Wong, “A robust dead-reckoning pedestrian tracking system with low cost sensors,” in *Proceedings of the 9th IEEE International Conference on Pervasive Computing and Communications (PerCom ’11)*, 2011, pp. 222–230.

[11] T. Higuchi, H. Yamaguchi, and T. Higashino, “Clearing a crowd: Context-supported neighbor positioning for people-centric navigation,” in *Proceedings of the 10th International Conference on Pervasive Computing (Pervasive ’12)*, 2012, (accepted).

[12] Y. F. Yiguang Xuan, Raja Sengupta, “Crowd sourcing indoor maps with mobile sensors,” in *Proceedings of the 7th International ICST Conference on Mobile and Ubiquitous Systemse (MobiQuitous ’10)*, 2010.

[13] Y. Wang, J. Gao, and J. S. Mitchell, “Boundary recognition in sensor networks by topological methods,” in *Proceedings of the 12th Annual International Conference on Mobile Computing and Networking (MobiCom ’06)*, 2006, pp. 122–133.

[14] G. Alessandretti, “Vehicle and guard rail detection using radar and vision data fusion,” *IEEE Transactions on Intelligent Transportation Systems*, vol. 8, no. 1, pp. 95–105, 2007.

[15] N. El-Sheimy, “The utilization of artificial neural networks for multisensor system integration in navigation and positioning instruments,” *IEEE Transactions on Instrumentation and Measurement*, vol. 55, no. 5, pp. 1606–1615, 2006.

[16] D. Smith and S. Singh, “Approaches to multisensor data fusion in target tracking: A survey,” *IEEE Transactions on Knowledge and Data Engineering*, vol. 18, pp. 1696–1710, 2006.

[17] X. Hong, C. Nugent, M. Mulvenna, S. McClean, B. Scotney, and S. Devlin, “Evidential fusion of sensor data for activity recognition in smart homes,” *Pervasive and Mobile Computing*, vol. 5, no. 3, pp. 236–252, 2009.

[18] D. Hall, “An introduction to multisensor data fusion,” *Proceedings of the IEEE*, vol. 85, no. 1, pp. 6–23, 1997.

[19] J. Kittler and F. M. Alkoot, “Sum versus vote fusion in multiple classifier systems,” *IEEE Transactions on Pattern Analysis and Machine Intelligence*, vol. 25, no. 1, pp. 110–115, 2003.

[20] Scalable Network Technologies, “QualNet (online).” [Online]. Available: http://www.scalable-networks.com/products/qualnet/

[21] Remcom, “Wireless InSite (online).” [Online]. Available: http://www.remcom.com/wireless-insite

[22] J. Parsons, *The mobile radio propagation channel*. Wiley, 1992.